Using a Multiobjective Approach to Compare Multiple Design Alternatives—An Application to Battery Dynamic Model Tuning

Alberto Pajares *, Xavier Blasco, Juan Manuel Herrero and Raúl Simarro

Instituto Universitario de Automática e Informática Industrial (ai2), Universitat Politècnica de València, Camí de Vera s/n, 46022 València, Spain; xblasco@upv.es (X.B.); juaherdu@upv.es (J.M.H.); rausifer@upv.es (R.S.)

* Correspondence: alpafer1@upv.es; Tel.: +34-963-877-000 (ext. 75713)

Abstract: A design problem is usually solvable in different ways or by design alternatives. In this work, the term "concept" is used to refer to the design alternatives. Additionally, it is quite common that a design problem has to satisfy conflicting objectives. In these cases, the design problem can be formulated as a multiobjective optimization problem (MOP). One of the aims of this work was to show how to combine multiobjective requirements with concepts' comparisons, in order to attain a satisfactory design. The second aim of this work was to take advantage of this methodology to obtain a battery model that described the dynamic behavior of the main electrical variables. Two objectives related to the model accuracy during the charge and discharge processes were used. In the final model selection, three different concepts were compared. These concepts differed in the complexity of their model structure. More complex models usually provide a good approximation of the process when identification data are used, but the approximation could be worse when validation data are applied. In this article, it is shown that a model with an intermediate complexity supplies a good approximation for both identification and validation data sets.

Keywords: multiobjective optimization; concept evaluation; battery model

---

1. Introduction

Many technical problems have different possible solutions and it is not always obvious which one is the best. In the literatures [1,2], these viable solutions are called "concepts". In this context, a multiobjective optimization approach can help designers with the decision-making process. As an example of an application of this methodology, this work explored the development and tuning of a dynamic model for an electric battery. When it comes to finding a range of feasible models, different techniques can be applied [3]. For instance, the model can be built by using a fuzzy approach [4], neural networks [5], first principles [6], etc. Each alternative may have its advantage or different degrees of approximation, depending on the scenario. Proposing concepts allows us to compare different model structures, and to choose the best one according to the designer preferences. For the designer, a framework where all the alternatives can be directly compared supplies valuable information for determining the final solution. A natural framework is the multiobjective optimization approach. Each concept has to satisfy conflicting design objectives, and it is in relation to these objectives that they have to be compared.

A multiobjective optimization problem (MOP) [7–9] deals with multiple design objectives, optimizing all of them simultaneously [10]. The solution to these types of problems is not unique. In fact, there is a set of optimal solutions, named the Pareto set, [11], and each solution of this set has a different trade-off between the design objectives. When these solutions are represented in the space of

objectives, they are collectively known as the Pareto front. Normally, it is not possible to find a single solution to optimize all the design objectives simultaneously, so the final solution must be selected from this set of optimal solutions by using a posteriori designer preferences [12].

Therefore, a multiobjective approach provides the possibility to compare and analyze the performance of different concepts against the selected objectives simultaneously [13,14]. In this way, we can obtain different Pareto fronts (one for each concept), in order to decide which one is the most convenient solution for the designer. In a traditional MOP, we can choose a solution from the Pareto front. By introducing concepts, it is possible to compare totally different types of solutions that share the same objectives, and to choose among them.

In this work, the battery of an electric vehicle prototype was modeled. The battery provided the energy, and its performance had a significant effect on the electrical behavior of the vehicle. The vehicle contained batteries of a lead acid gel type (Haze HZY12-33, 12V).

Many types of battery models have been presented so far in the literature: models based on first principles [6], simple [15] and complex models [16], linear and nonlinear models [17], models based on fuzzy logic [18] and on neural networks [19], and generic models [20]. A good battery model for a vehicle should describe the charge process as well as the discharge process. Thus, in this paper, both dynamics were integrated into a single model.

For control design and energy management purposes, it is not necessary to increase a model's complexity excessively. After a certain degree of complexity, the improvement in performance is negligible. Consequently, it is interesting to analyze the performance improvement when adding complexity in a model [17,21]. We believed that the use of a multiobjective approach to compare concepts could be very helpful to analyze the trade-off between complexity and performance for different battery model structures.

The following is a brief outline of the research methodology followed in this study. First, a series of tests were carried out, in order to identify the battery behavior during its charging and discharging at several currents (within the range of more usual currents). Secondly, three different battery model structures were proposed as possible solutions. These three structures differed in complexity. For each structure, it is highlighted which parameters had to be adjusted. Then, this adjustment (for each structure) was performed by solving a MOP, with two objectives to minimize at the same time. Both of these measured the model performance, but in two different state of charge (SOC) intervals. Finally, an analysis of the Pareto fronts obtained for each of the three battery model structures enabled us to compare them.

Additionally, in order to give some degree of robustness, the results from the validation process were also taken into account in the comparison. This supplied valuable information about the performance degradation for each concept. All this information was very useful for making the decision about which structure was the most suitable, and which adjustment of the parameters was finally chosen.

The article is structured as follows. In Section 2, the experimental tests for identification are presented. In Section 3, the battery model structures are defined. Section 4 presents the MOP for the model identification. In Section 5, the results are shown. Finally, the conclusions are commented on.

2. Experimental Tests

In this work, a lead acid gel type battery (Haze HZY12-33, 12V) was used. In order to identify the model parameters, it was necessary to do a set of experimental tests. Three discharge tests, at low I_l, medium I_m and high I_h currents, were performed. These three currents were taken from the manufacturer data sheet. They corresponded to the currents that discharged the battery in 20 h ($I_l = 1.57$ A, used in test 1; see Figure 1), 2 h ($I_m = 10.2$ A, used in test 2; see Figure 2) and 0.5h ($I_h = 29.6$ A, used in test 3; see Figure 3).

In addition, two charge tests, at two different currents, were carried out. These charge currents were $I_{c1} = -2$ A, used in test 4 (see Figure 4), and $I_{c2} = -4$ A, for test 5 (see Figure 5). All these tests (tests 1 to 5) were used in the identification process of the models.

In the discharge tests, the current extracted from the battery was a square signal. The result was a repetitive sequence composed of discharge zones (DZs; where a constant current was extracted from the battery until the capacity at that current fell by 10%), followed by rest zones (RZs; 2 h), as is shown in Figure 1 [16,22,23]. The RZs were used to know the open circuit voltage of the battery at different SOCs.

In the charge tests, a constant current was applied to the battery until its voltage reached 13.7 V (manufacturer's recommendation), as is shown in Figure 4. Next, the current was turned off, and the battery rested to the end of the test. In this way, we charged the battery up to approximately 90%. As a result, these tests also had two different zones, the charge zone (CZ) and the RZ.

Moreover, based on the evolution of the battery SOC during each test, three additional zones are differentiated in the figures: $Zone_{LSOC}$, $Zone_{MSOC}$ and $Zone_{HSOC}$. These indicate when the battery capacity at the required current was low (below 20%), medium (between 20% and 80%) or high (above 80%). These SOC zones serve to discriminate between the performance of the model in the most common zones of work ($Zone_{MSOC}$) and the least common ($Zone_{LSOC}$ and $Zone_{HSOC}$). This helped us to define the objectives of the MOP in Section 4.2.

After observing the experimental tests, we noticed some details related to the battery behavior that we wanted to take into account in the dynamic model of the battery. First, when a discharge current was applied, a voltage drop occurred, and the voltage drop/current ratio depended on the SOC and the current. Second, the slope of the voltage drop in the DZ also depended on the SOC and the current.
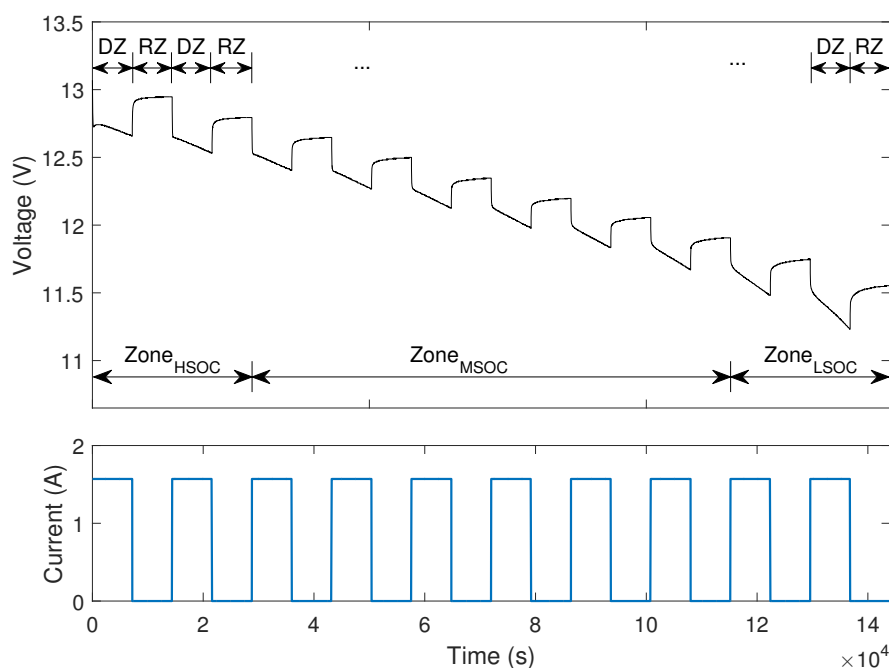

Figure 1. Battery discharge response in test 1 ($I = I_l = 1.57$ A). Rest zones (RZs) correspond to time intervals when the current was zero, and discharge zones (DZs) are the remaining time intervals (discharge times). $Zone_{HSOC}$, $Zone_{MSOC}$ and $Zone_{LSOC}$ are the zones at high, medium and low SOCs, respectively.
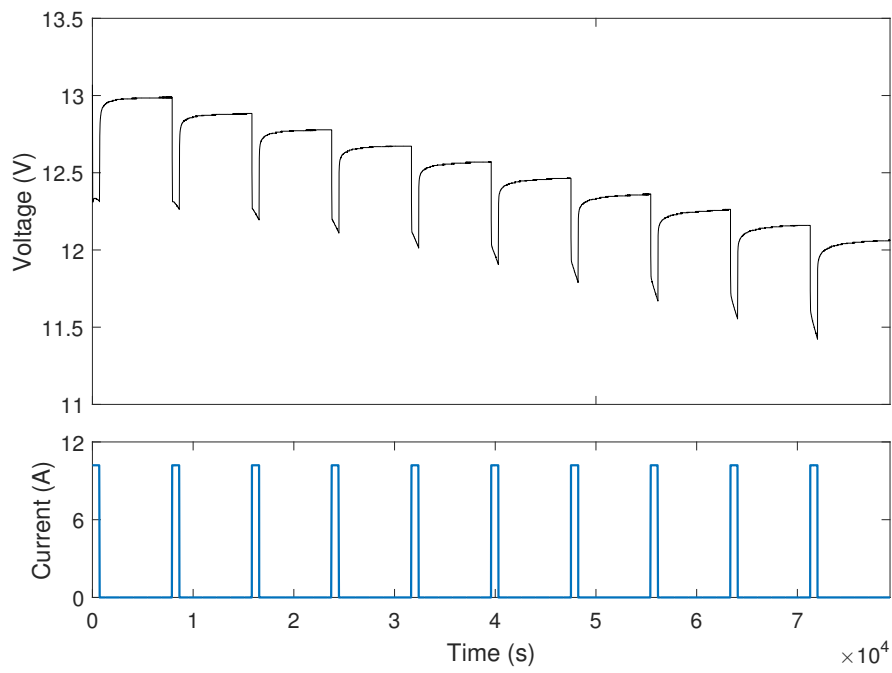
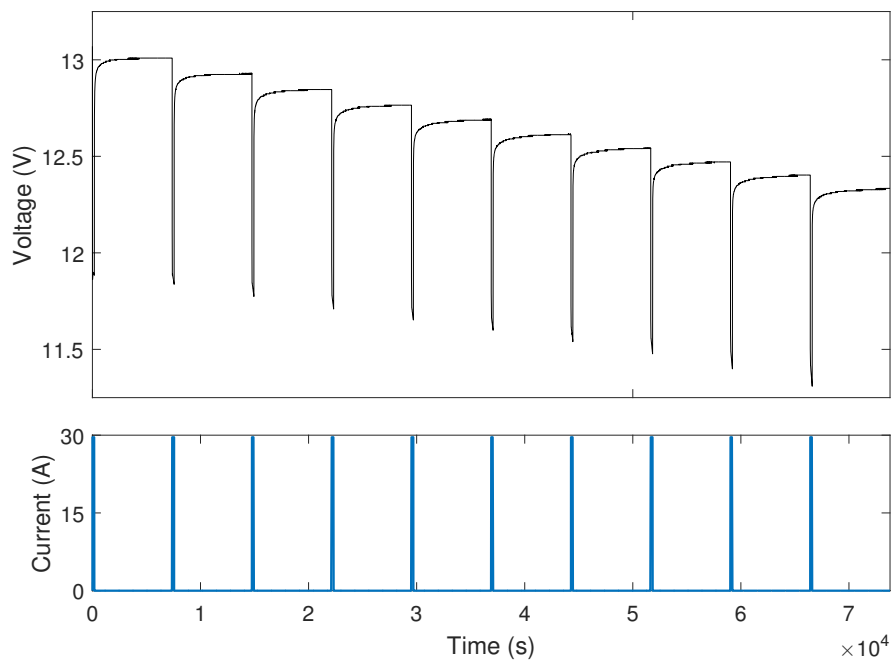**Figure 2.** Battery discharge response in test 2 ($I = I_m = 10.2$ A).

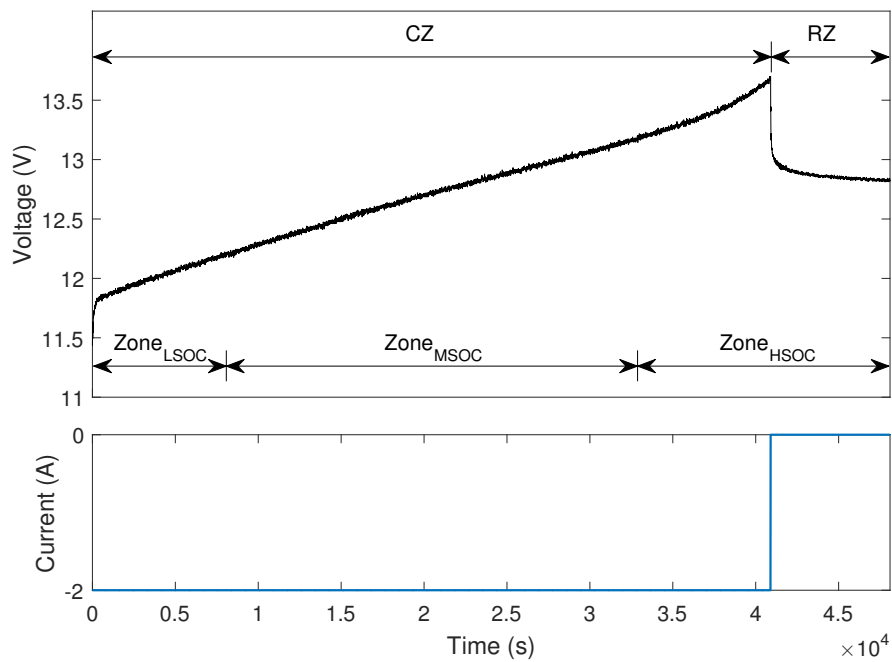**Figure 3.** Battery discharge response in test 3 ($I = I_h = 29.6$ A).

Figure 4. Battery charge response in test 4 ($I = I_{c1} = -2$ A). RZ corresponds to the time interval when the current was zero, and CZ (charge zone) is the remaining time interval (charge time). $Zone_{HSOC}$, $Zone_{MSOC}$ and $Zone_{LSOC}$ are the zones at high, medium and low SOCs, respectively.

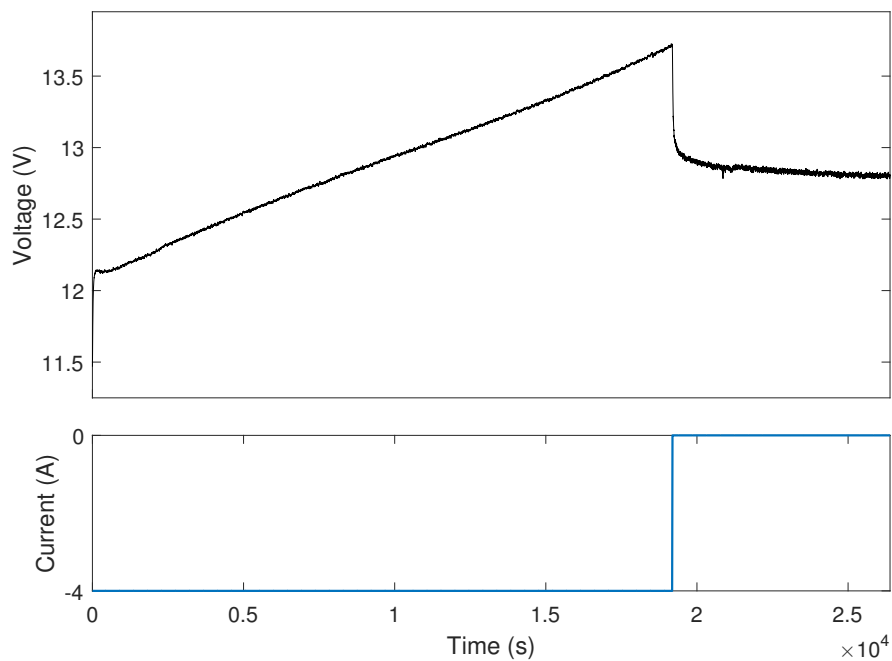**Figure 5.** Battery charge response in test 5 ($I = I_{c2} = -4$ A).

3. Dynamic Models of the Battery

This section presents three different structures of the battery model. Each one represents a concept (see Figure 6). Table 1 shows all the parameters used in these models. Structure (a) is the complete model and the first concept (C_1). Structure (b) is the intermediate model (second concept, C_2), and it is

a simplification of the complete model. The simple model (third concept, C_3) is structure (c), and it is a simplification of the intermediate model.
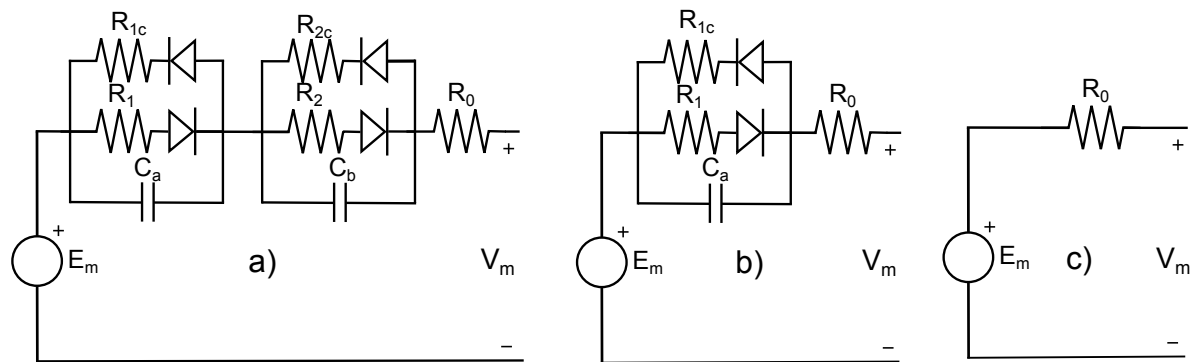

Figure 6. Battery model structures: (**a**) complete model (C_1), (**b**) intermediate model (C_2), and (**c**) simple model (C_3).

Table 1. Table of symbols. The parameters in bold are the estimated parameters.

Parameter	Description	Value	Unit
I	Battery current (input)	-	A
T_b	Battery temperature (input)	-	°C
Em_0	Open-circuit voltage at full charge	13.1	V
K_e	Constant, which depends on $\mathbf{K^c_e}$, $\mathbf{K^l_e}$, $\mathbf{K^m_e}$ and $\mathbf{K^h_e}$	-	V/°C
K_c	Constant	1.24	-
C^*_0	No-load capacity at 0 °C	25.62	Ah
δ	Constant	0.64	-
ϵ	Constant	0.34	-
I_{nom}	Nominal battery current	1.57	A
T_f	Electrolyte freezing temperature	−40	°C
R_0	Resistor, whose value depends on $\mathbf{R^l_{00}}$, $\mathbf{R^m_{00}}$, $\mathbf{R^h_{00}}$, $\mathbf{A^l_0}$, $\mathbf{A^m_0}$ and $\mathbf{A^h_0}$	-	Ω
R_1	First RC resistor, whose value depends on $\mathbf{R_{11}}$, $\mathbf{R_{12}}$, $\mathbf{R_{13}}$, $\mathbf{R_{14}}$, $\mathbf{R_{15}}$ and $\mathbf{R_{16}}$	-	Ω
R_{1c}	First RC resistor, whose value depends on $\mathbf{R_{17}}$ and $\mathbf{R_{18}}$	-	Ω
R_2	Second RC resistor, whose value depends on $\mathbf{R_{21}}$, $\mathbf{R_{22}}$ and $\mathbf{R_{23}}$	-	Ω
$\mathbf{R_{2c}}$	Resistor of the second RC circuit	-	Ω
$\mathbf{C_a}$	First RC capacitor	-	F
$\mathbf{C_b}$	Second RC capacitor	-	F
I_l	When $I \leq I_l$ & $I > 0$, this is considered a low current	1.57	A
I_m	When $I \leq I_m$ & $I > I_l$, this is considered a medium current	10.2	A
I_h	When $I \leq I_h$ & $I > I_m$, this is considered a high current	29.6	A
I_{c1}	First charge current	−2	A
I_{c2}	Second charge current	−4	A
$SOC_{verylow}$	When $SOC \leq SOC_{verylow}$, this is considered a very low SOC	20	%
SOC_{low}	When $SOC \leq SOC_{low}$ & $SOC > SOC_{verylow}$: low SOC	37.5	%
SOC_{medium}	When $SOC \leq SOC_{medium}$ & $SOC > SOC_{low}$: medium SOC	55	%
SOC_{high}	When $SOC \leq SOC_{high}$ & $SOC > SOC_{medium}$: high SOC	90	%

3.1. Complete Model

In this model (Figure 6, structure (a)), the battery voltage V_m is the output, whose dynamic behavior depended on the initial SOC, the temperature (T_b) and the current (I). The model had a voltage source, five resistors and two capacitors. This model did not include the losses that occurred at the end of the battery charge (SOC near 100%), as it was not considered to be a relevant situation and its inclusion would only have added unnecessary complexity to the model.

3.1.1. Open Circuit Voltage

The open circuit voltage of the model E_m is defined by Equation (1) [24,25]:

$$E_m = E_{m0} - K_e(273 + T_b)(1 - SOC) \tag{1}$$

where E_{m0} is the open circuit voltage when the battery was fully charged, T_b is the temperature of the battery in $°C$, SOC is the state of charge of the battery, and K_e (see Equation (2) and Figure 7) is a parameter that depends on the current, as it was observed in the experimental tests of the previous section. This parameter could be identified for the currents used in the identification tests. Between them, a linear interpolation was carried out, which, as can be seen from the validation test, produced good results.
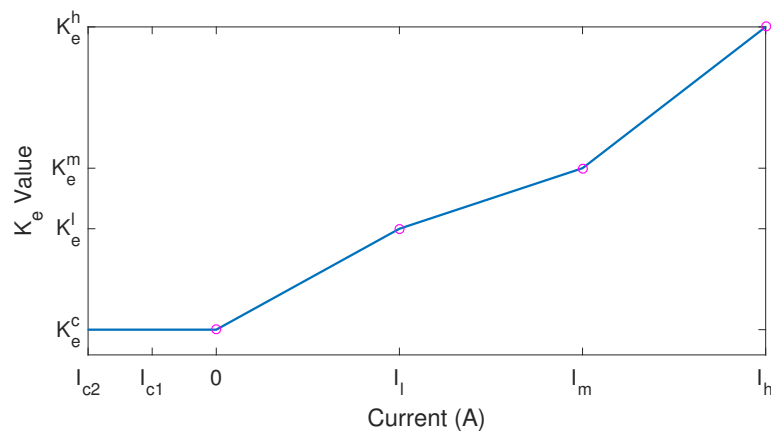

Figure 7. Graphical representation of the parameter K_e. I_{c1} and I_{c2} are charge currents (negative values) and I_l, I_m and I_h (positive values) are discharge currents used in the identification process.

$$K_e = \begin{cases} K_e^h & \text{if} \quad I > I_h \\ \frac{K_e^h - K_e^m}{I_h - I_m}(I - I_m) + K_e^m & \text{if} \quad I > I_m \quad and \quad I \leq I_h \\ \frac{K_e^m - K_e^l}{I_m - I_l}(I - I_l) + K_e^l & \text{if} \quad I > I_l \quad and \quad I \leq I_m \\ \frac{K_e^l - K_e^c}{I_l}(I) + K_e^c & \text{if} \quad I > 0 \quad and \quad I \leq I_l \\ K_e^c & \text{if} \quad I \leq 0 \end{cases} \tag{2}$$

where I is the current of the battery; I_h, I_m and I_l are the high, medium and low currents, respectively; and K_e^h, K_e^m, K_e^l and K_e^c are estimated parameters.

3.1.2. State of Charge

The SOC is a vital part for the operation of a battery model. The SOC indicates the capacity available in the battery. The capacity available $C(I, T_b)$ depends on the discharge currents, and is modeled as [24,25]:

$$C(I, T_b) = \frac{K_c C_0^*}{1 + (K_c - 1)(\frac{I}{I_{nom}})^\delta}(1 + \frac{T_b}{T_f})^\epsilon \tag{3}$$

where K_c, δ and ϵ are estimated parameters; C_0^* is the capacity of the battery at $0 °C$; I_{nom} is the nominal current; and T_f is the electrolyte freezing temperature. Therefore, the SOC of the battery [24,25] (in Ah) is defined as follows:

$$SOC = 1 - \int \frac{I}{3600\, C(0, T_b)} \tag{4}$$

The values for C_0^*, ϵ, K_c and δ were taken from the manufacturer's data sheet.

3.1.3. Resistance R_0

The instantaneous voltage drop, caused by changes in the current, is modeled through the resistance R_0 [24,25]. As we saw in the experimental tests in the previous section, this voltage drop depends on the SOC and the current. Therefore, in order to model this resistance, the following equation is used:

$$R_0 = R_{00}[1 + A_0(1 - SOC)] \tag{5}$$

where R_{00} and A_0 (see Equations (6) and (7), and Figures 8 and 9) are parameters that depend on the current.
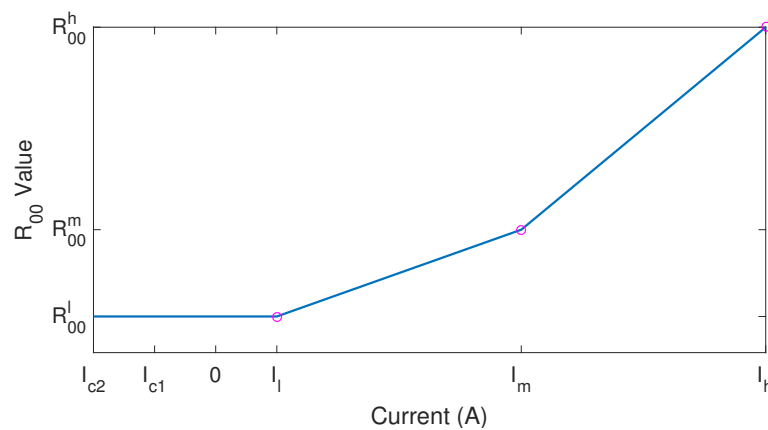
Figure 8. Graphical representation of R_{00}.

$$R_{00} = \begin{cases} R_{00}^h & \text{if} \quad I > I_h \\ \frac{R_{00}^h - R_{00}^m}{I_h - I_m}(I - I_m) + R_{00}^m & \text{if} \quad I > I_m \quad and \quad I < I_h \\ \frac{R_{00}^m - R_{00}^l}{I_m - I_l}(I - I_l) + R_{00}^l & \text{if} \quad I > I_l \quad and \quad I < I_m \\ R_{00}^l & \text{if} \quad I \leq I_l \end{cases} \tag{6}$$
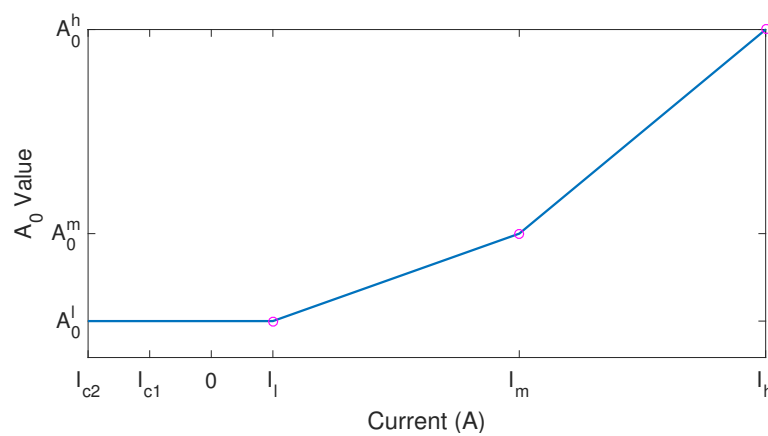
Figure 9. Graphical representation of A_0.

$$A_0 = \begin{cases} A_0^h & \text{if} \quad I > I_h \\ \frac{A_0^h - A_0^m}{I_h - I_m}(I - I_m) + A_0^m & \text{if} \quad I > I_m \quad and \quad I \leq I_h \\ \frac{A_0^m - A_0^l}{I_m - I_l}(I - I_l) + A_0^l & \text{if} \quad I > I_l \quad and \quad I \leq I_m \\ A_0^l & \text{if} \quad I \leq I_l \end{cases} \tag{7}$$

where R_{00}^h, R_{00}^m, R_{00}^l, A_0^h, A_0^m and A_0^l are estimated parameters. These parameters could be identified for the currents used in the experimental tests. Again, between these values, a linear interpolation was carried out, which produced good results in the validation test. (An initial test showed a significant performance degradation when a linear regression was used for the parameters K_e, R_{00} and A_0, in comparison with a piecewise linear approximation proposed.) In order to limit the number of parameters, in the charge process (currents I_{c1} and I_{c2}), both R_{00} and A_0 were set to the values of low currents R_{00}^l and A_0^l, respectively. This selection supplied an adequate approximation.

3.1.4. First RC Circuit (R_1, R_{1c} and C_a)

The RC circuit formed by the resistances R_1 and R_{1c} and the capacitor C_a incorporated the main dynamics of the model. Resistance R_1 influenced the model response only during the discharge process, whereas R_{1c} influenced only in the charge process. It has been observed experimentally that the value of R_1 depends on the current and the SOC. Therefore, R_1 is defined in Table 2 (using a bilinear interpolation).

Table 2. Lookup table for R_1. R_{11}, R_{12}, R_{13}, R_{14}, R_{15} and R_{16} are estimated parameters.

	SOC	
	High	**Very Low**
High Current, I_h	R_{11}	R_{12}
Medium Current, I_m	R_{13}	R_{14}
Low Current, I_l	R_{15}	R_{16}

On the other hand, it has been observed experimentally that the value of R_{1c} depends on the current, but not on the SOC. Thus, R_{1c} is defined by Equation (8):

$$R_{1c} = R_{17}I + R_{18} \tag{8}$$

where R_{17} and R_{18} are estimated parameters. Finally, the value of the capacitor C_a is also an estimated parameter.

3.1.5. Second RC Circuit (R_2, R_{2c} and C_b)

This part of the model aimed at adjusting the behavior of the battery when it was near the end of its capacity, having no influence in any other case. This capacity depended on the discharge current (see Equation (3)). According to the data sheet, it was not possible to reach a low or very low SOC at a high discharge current. Moreover, it was not possible to reach a very low SOC at a medium current. R_2 was defined by a bilinear interpolation (see Table 3). The resistance R_{2c} and the capacitor C_b were estimated constants.

Table 3. Lookup table for R_2. R_{21}, R_{22} and R_{23} are estimated parameters.

	SOC			
	High	**Medium**	**Low**	**Very Low**
High Current	0	R_{21}	-	-
Medium Current	0	0	R_{22}	-
Low Current	0	0	0	R_{23}

For convenience, the estimated parameters were separated into three different vectors ($\boldsymbol{\theta_1}$, $\boldsymbol{\theta_2}$ and $\boldsymbol{\theta_3}$). $\boldsymbol{\theta_1}$ contained the parameters to be estimated in the three proposed models; $\boldsymbol{\theta_2}$, only those that were common to both the complete and intermediate models; and $\boldsymbol{\theta_3}$ consisted of the parameters to be estimated only in the complete model.

$$\boldsymbol{\theta_1} = (K_e^h, K_e^m, K_e^l, K_e^c, R_{00}^h, R_{00}^m, R_{00}^l, A_0^h, A_0^m, A_0^l) \tag{9}$$

$$\boldsymbol{\theta_2} = (R_{11}, R_{12}, R_{13}, R_{14}, R_{15}, R_{16}, R_{17}, R_{18}, C_a) \tag{10}$$

$$\boldsymbol{\theta_3} = (R_{21}, R_{22}, R_{23}, R_{2c}, C_b) \tag{11}$$

3.2. Intermediate Model

The intermediate model was a simplification of the complete model, which has been described previously. This intermediate model was the same as the complete model, except that the second RC circuit had been removed. For this reason, this model did not have the possibility to accurately adjust the battery voltage when the battery was near the end of its capacity. This model had 19 parameters to estimate ($\boldsymbol{\theta_1}$ and $\boldsymbol{\theta_2}$; see Figure 6, structure (b)).

3.3. Simple Model

The simple model was a simplification of the intermediate model, which has been described previously. This simple model was the same as the intermediate model, except that the first RC circuit had been removed. Thus, this model had 10 parameters to estimate ($\boldsymbol{\theta_1}$; see Figure 6, structure (c)).

4. Multiobjective Optimization Problem For Electrical Model Identification

4.1. Decision Space

Three concepts have been defined; each one had a different set of parameters to identify (see Section 3). In order to set a MOP, the objectives and the decision variables of the problem have to be defined [26]. The decision variables of the first concept (C_1) were the 24 parameters defined in Section 3.1, which composed the vector θ^{c1}. The decision variables of the second concept (C_2) were the 19 parameters defined in Section 3.2, which composed the vector θ^{c2}. Finally, the decision variables of the third concept (C_3) were the 10 parameters defined in Section 3.3, which composed the vector θ^{c3}.

$$\theta^{c1} = [\boldsymbol{\theta_1}, \boldsymbol{\theta_2}, \boldsymbol{\theta_3}] \tag{12}$$

$$\theta^{c2} = [\boldsymbol{\theta_1}, \boldsymbol{\theta_2}] \tag{13}$$

$$\theta^{c3} = [\boldsymbol{\theta_1}] \tag{14}$$

The approximate values of some parameters were known (these were presented in Section 2). By observing the correct operating range of the rest of the parameters, their lower and higher limits were established. These limits are shown in Table 4.

Table 4. Parameter search space.

	$\underline{K}_e^h$	0.004		$\overline{K}_e^h$	0.0075
	$\underline{K}_e^m$	0.0052		$\overline{K}_e^m$	0.008
	$\underline{K}_e^l$	0.0045		$\overline{K}_e^l$	0.0075
	$\underline{K}_e^c$	0.0075		$\overline{K}_e^c$	0.015
$\underline{\theta}_1$	$\underline{R}_{00}^h$	0.008	$\overline{\theta}_1$	$\overline{R}_{00}^h$	0.23
	$\underline{R}_{00}^m$	0.019		$\overline{R}_{00}^m$	0.07
	$\underline{R}_{00}^l$	0.035		$\overline{R}_{00}^l$	0.25
	$\underline{A}_{00}^h$	0.05		$\overline{A}_0^h$	0.7
	$\underline{A}_{00}^m$	0.1		$\overline{A}_0^m$	1.65
	$\underline{A}_{00}^l$	0.35		$\overline{A}_0^l$	1.9
	$\underline{R}_{11}$	0.0065		$\overline{R}_{11}$	0.0225
	$\underline{R}_{12}$	1e-5		$\overline{R}_{12}$	1e-3
	$\underline{R}_{13}$	0.01		$\overline{R}_{13}$	0.04
	$\underline{R}_{14}$	1e-4		$\overline{R}_{14}$	0.0035
$\underline{\theta}_2$	$\underline{R}_{15}$	0.08	$\overline{\theta}_2$	$\overline{R}_{15}$	0.2
	$\underline{R}_{16}$	0.008		$\overline{R}_{16}$	0.04
	$\underline{R}_{17}$	-0.0065		$\overline{R}_{17}$	-0.045
	$\underline{R}_{18}$	0.31		$\overline{R}_{18}$	0.45
	$\underline{C}_a$	750		$\overline{C}_a$	2000
	$\underline{R}_{21}$	1.15		$\overline{R}_{21}$	1.75
	$\underline{R}_{22}$	0.022		$\overline{R}_{22}$	0.05
$\underline{\theta}_3$	$\underline{R}_{23}$	0.075	$\overline{\theta}_3$	$\overline{R}_{23}$	0.55
	$\underline{R}_{2c}$	0.025		$\overline{R}_{2c}$	0.045
	$\underline{C}_b$	1.5e5		$\overline{C}_b$	2.5e5

$$\underline{\theta}^{c1} = [\underline{\theta}_1, \underline{\theta}_2, \underline{\theta}_3] \tag{15}$$

$$\overline{\theta}^{c1} = [\overline{\theta}_1, \overline{\theta}_2, \overline{\theta}_3] \tag{16}$$

$$\underline{\theta}^{c2} = [\underline{\theta}_1, \underline{\theta}_2] \tag{17}$$

$$\overline{\theta}^{c2} = [\overline{\theta}_1, \overline{\theta}_2] \tag{18}$$

$$\underline{\theta}^{c3} = [\underline{\theta}_1] \tag{19}$$

$$\overline{\theta}^{c3} = [\overline{\theta}_1] \tag{20}$$

4.2. Objectives

In order to define the objectives, several aspects were considered. First, it was observed that the battery had a non-linear behavior, which depended on the SOC. For this reason, the adjustments of the simple and the intermediate models were expected to be less accurate than those of the complete model. A second consideration was that batteries, in most applications, operate in the medium SOC zone (this is typically the case in electric vehicle applications). Consequently, it seemed a reasonable

decision to define one of the objectives so that it measured the accuracy of the adjustment in that zone. This could have had an additional, plausible consequence, namely, that the simple and intermediate models may have been competitive enough.

From these considerations, two objectives were defined to include the conceivable specifications of a designer. Both objectives measured the performance of the model in two different SOC intervals. The first objective was the voltage error between the model and the experimental data in the zones of low and high SOC, whereas the second was of the same magnitude, but in the medium SOC zone. By comparing these two objectives, a designer could easily assess: (1) which concept worked better in each SOC zone, and (2) which solution, within a concept, worked better in each SOC zone. Moreover, this methodology would enable the designer to evaluate how the complexity of the model structure affected the performance in the different SOC zones.

The first objective (J_1, Equation (23)) evaluated the sum of differences between the V_m of the model and the battery voltage measurement at high and low SOCs in each test (ZHL), that is to say, zones $Zone_{HSOC}$ and $Zone_{LSOC}$ (tests $1-5$). The errors were normalized by dividing them by the duration of each zone, which provided an average error for the DZ or CZ and RZ time intervals. J_{ZHL}^D (discharge tests) and J_{ZHL}^C (charge tests) were the result of a weighted sum of both averages. Finally, J_1 (in volts) was calculated as an average of J_{ZHL}^D and J_{ZHL}^C for all of the experimental tests. As a result, all the intervals had the same relative importance.

$$J_{ZHL}^D(test_i) = 0.5 \sum_{DZ \in ZHL} \frac{|V_m - V_{test_i}|}{duration_{DZ}} + 0.5 \sum_{RZ \in ZHL} \frac{|V_m - V_{test_i}|}{duration_{RZ}} \tag{21}$$

$$J_{ZHL}^C(test_i) = 0.5 \sum_{CZ \in ZHL} \frac{|V_m - V_{test_i}|}{duration_{CZ}} + 0.5 \sum_{RZ \in ZHL} \frac{|V_m - V_{test_i}|}{duration_{RZ}} \tag{22}$$

$$J_1 = \frac{\sum_{i=1}^{3} J_{ZHL}^D(test_i) + \sum_{i=4}^{5} J_{ZHL}^C(test_i)}{Number\ of\ Tests} \tag{23}$$

The second objective J_2 (in V) was defined by Equation (26) in the same way as J_1, but it only took into account errors (in V) at the medium SOC in each test (ZM): $Zone_{MSOC}$ (tests $1-5$). J_{ZM}^D and J_{ZM}^C are the errors that occurred in the discharge and charge tests, respectively, both in ZM areas.

$$J_{ZM}^D(test_i) = 0.5 \sum_{DZ \in ZM} \frac{|V_m - V_{test_i}|}{duration_{CZ}} + 0.5 \sum_{RZ \in ZM} \frac{|V_m - V_{test_i}|}{duration_{RZ}} \tag{24}$$

$$J_{ZM}^C(test_i) = 0.5 \sum_{CZ \in ZM} \frac{|V_m - V_{test_i}|}{duration_{CZ}} + 0.5 \sum_{RZ \in ZM} \frac{|V_m - V_{test_i}|}{duration_{RZ}} \tag{25}$$

$$J_2 = \frac{\sum_{i=1}^{3} J_{ZM}^D(test_i) + \sum_{i=4}^{5} J_{ZM}^C(test_i)}{Number\ of\ Tests} \tag{26}$$

4.3. The Multiobjective Optimization Problem

Three different concepts [13] (C_1, C_2 and C_3) were considered when J_1 and J_2 were evaluated. The optimization problem for each concept was defined as:

$$C_1 \quad : \quad \min_{\overline{\theta}^{c1} \leq \theta^{c1} \leq \underline{\theta}^{c1}} (J_1, J_2) \tag{27}$$

$$C_2 \quad : \quad \min_{\overline{\theta}^{c2} \leq \theta^{c2} \leq \underline{\theta}^{c2}} (J_1, J_2) \tag{28}$$

$$C_3 \quad : \quad \min_{\overline{\theta}^{c3} \leq \theta^{c3} \leq \underline{\theta}^{c3}} (J_1, J_2) \tag{29}$$

Thus, three Pareto Fronts were obtained, one for each concept. The evolutionary multiobjective algorithm ev-MOGA [27] was used (ev-MOGA is available at Matlab file exchange: https://es.mathworks.com/matlabcentral/fileexchange/ 31080-ev-moga-multiobjective-evolutionary-algorithm). This algorithm has demonstrated a good performance in different design problems [28,29]. It characterizes the Pareto front in a distributed way, showing a wide variety of Pareto solutions to the designer. This smart distribution of the Pareto front helps the designer to analyze and to select the final solution in a better way. The ev-MOGA setting was the following: the number of individuals of the population (P) was 1000, and the number of iterations was 1000. The rest of the parameters were left at their default values.

5. Results and Evaluation

In Figure 10, the three Pareto fronts belonging to each one of the three concepts are depicted. As expected, the fronts did not conflict with each other because C_3 was a simplification of C_2, which was, in turn, a simplification of C_1. On the one hand, it was observed that the Pareto front of C_1 dominated the Pareto front of C_2, and the latter dominated the Pareto front of C_3. On the other hand, it was also observed that the performances were significantly worse in C_3, but this did not happen in C_2. In addition, the objective J_2 presented similar values in C_1 and C_2. Our first conclusion, therefore, was that it was worth discarding C_3, as its performances were significantly worse than the other concepts'.
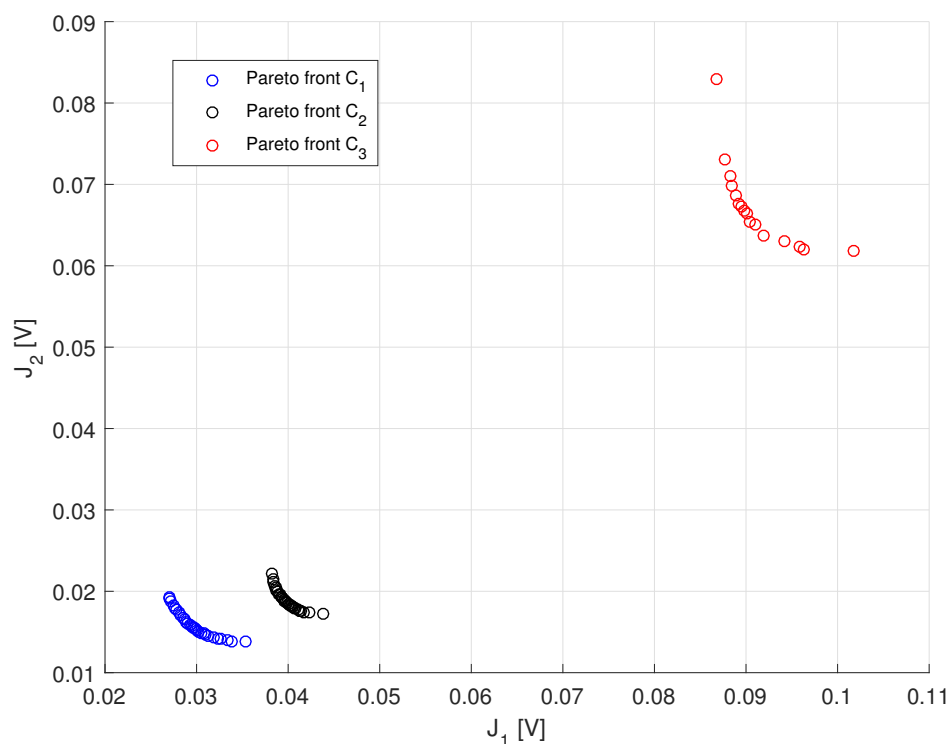

Figure 10. C_1, C_2 and C_3 Pareto fronts.

In Figure 11, the fronts corresponding to C_1 and C_2 are shown in detail. The models corresponding to the Pareto front extremes and the compromise solution—that with the least distance to the utopic solution (the minimum values of J_1 and J_2) using the 2-norm—are highlighted.

As an example, in Figure 12, the responses of these models in different SOC intervals are plotted and compared with the empirical data of test 1. Plots (a), (b) and (c) show the responses of the concept C_1, whereas the responses of the concept C_2 are shown in (d), (e) and (f). As mentioned, each plot corresponded to a different SOC zone. For instance, plots (a) and (d) corresponded to $Zone_{HSOC}$. The

extreme solutions of the different fronts performed very well for one of the objectives. This fact can be observed for solutions $\theta_{J_2}^{C_1}$ and $\theta_{J_2}^{C_2}$; they were the best in the $Zone_{MSOC}$, but the worst in the $Zone_{LSOC}$ for the intermediate model and $Zone_{HSOC}$ for the complete model. On the other hand, $\theta_{J_1}^{C_1}$ and $\theta_{J_1}^{C_2}$ were the best in ZHL. Finally, the solutions $\theta_{comp}^{C_1}$ and $\theta_{comp}^{C_2}$ provided a more a balanced performance. Note that $\theta_{comp}^{C_1}$ and $\theta_{comp}^{C_2}$ were not the only solutions that displayed a balanced performance, but initially we preferred them. It was also observed that when the SOC was low, the accuracy of C_2 deteriorated. This was because the second RC block was responsible for adjusting this zone, and this model did not include it. Regardless, neither C_1 nor C_2 could adjust the voltage in any SOC zone, as there were unmodeled dynamics.
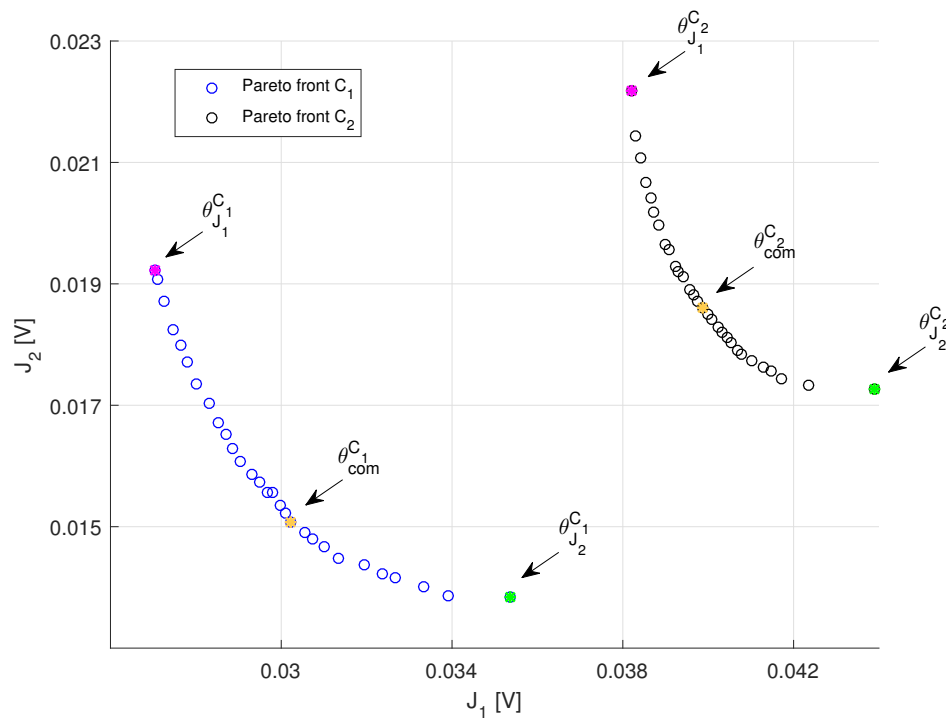

Figure 11. C_1 and C_2 Pareto fronts. The extreme solutions and the compromise solutions—those with the least distance to the utopic solution (the minimum values of J_1 and J_2) using the 2-norm—are highlighted.
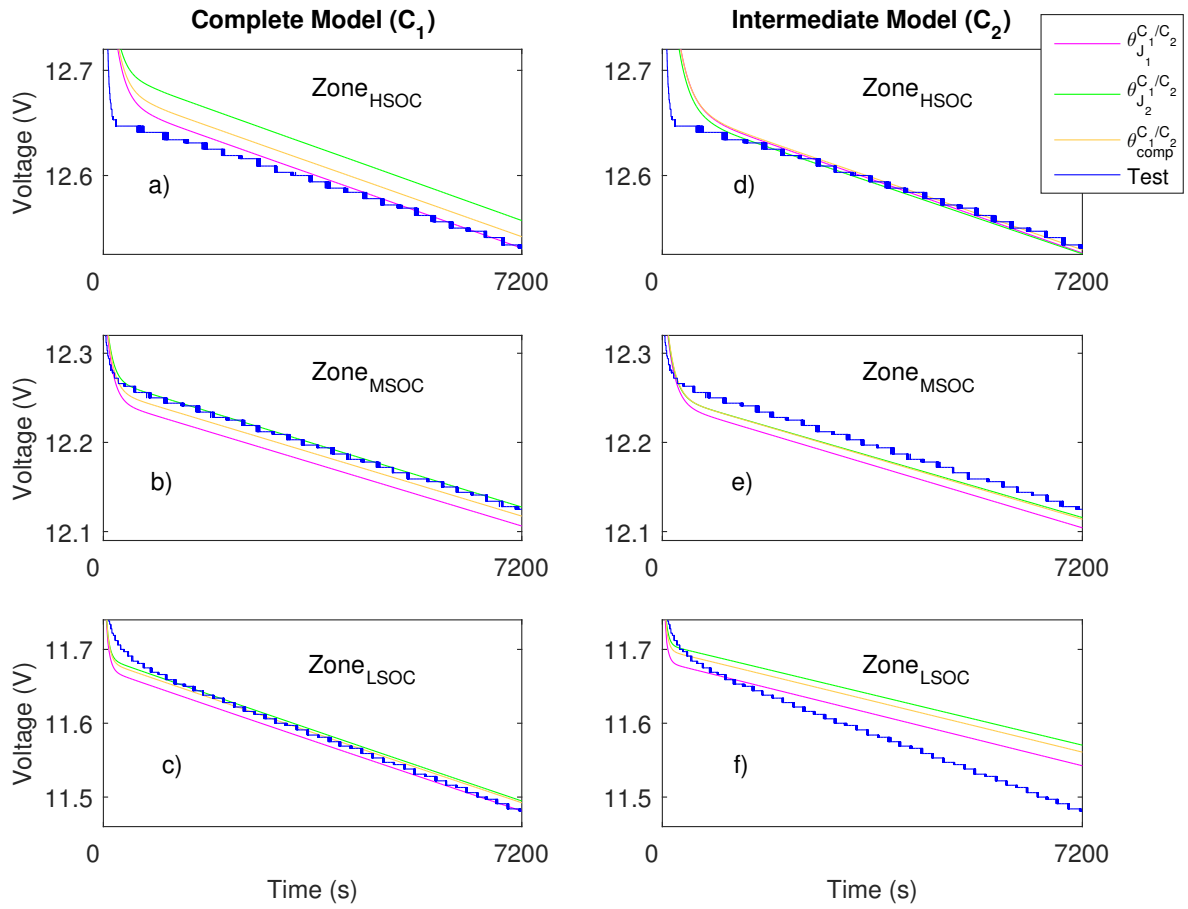
Figure 12. Discharge responses of the solutions highlighted in Figure 11 in different SOC zones, compared with the empirical data from test 1.

In order to analyze the robustness of each model in the Pareto fronts, a validation test was carried out (see Figure 13). Here, the performance of each model was assessed by means of J_1^{val} and J_2^{val}, both in volts (these were the equivalents to the objectives J_1 and J_2 presented in the MOP, but for the validation test). This test had neither CZs nor RZs.

$$J_{ZHL}^D(test_{val}) = \sum_{DZ \in ZHL} \frac{|V_m - V_{test_{val}}|}{duration_{DZ}} \tag{30}$$

$$J_1^{val} = J_{ZHL}^D(test_{val}) \tag{31}$$

$$J_{ZM}^D(test_{val}) = \sum_{DZ \in ZM} \frac{|V_m - V_{test_{val}}|}{duration_{DZ}} \tag{32}$$

$$J_2^{val} = J_{ZM}^D(test_{val}) \tag{33}$$

Figure 14 compares the performance of the solutions of the Pareto fronts that were obtained in the identification test with the performance that these solutions displayed in the validation test. The solutions of the Pareto fronts were the best solutions according to the identification tests, however, it is evident that they were not the best solutions according to the validation test. Thus, in the validation test, the performance of these solutions deteriorated, as expected. An additional observation was

that, in the validation test, some solutions in C_2 displayed a better performance (with respect to both objectives) than some solutions in C_1. After taking into account the results from the validation test, we concluded that the θ_{val}^{C1} and θ_{val}^{C2} models (highlighted in Figure 14) were better choices, as they were optimal solutions—they belonged to the Pareto front obtained with the identification data—and also exhibited a balanced performance (as θ_{comp}^{C1} and θ_{comp}^{C2} did). Additionally, they had a better performance in the validation test when compared to θ_{comp}^{C1} and θ_{comp}^{C2}.
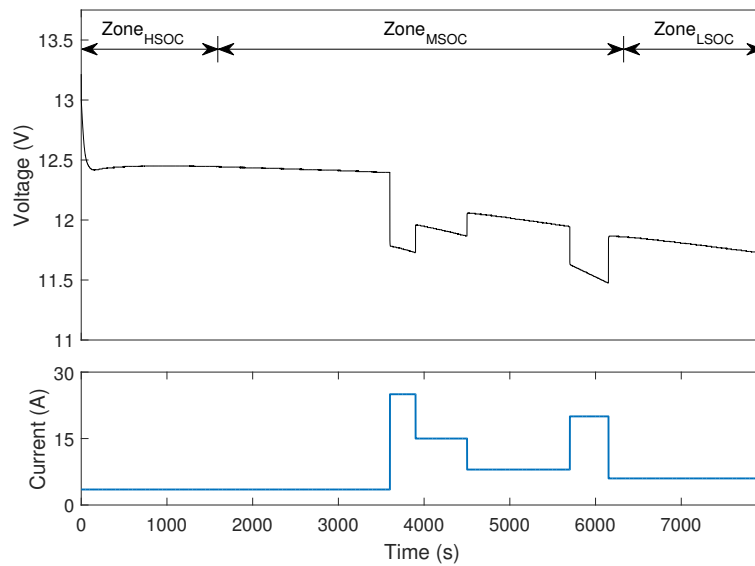
Figure 13. Experimental data from the validation test. The whole test took place in a DZ. $Zone_{HSOC}$, $Zone_{MSOC}$ and $Zone_{LSOC}$ correspond to the zones with high, medium and low SOC, respectively.
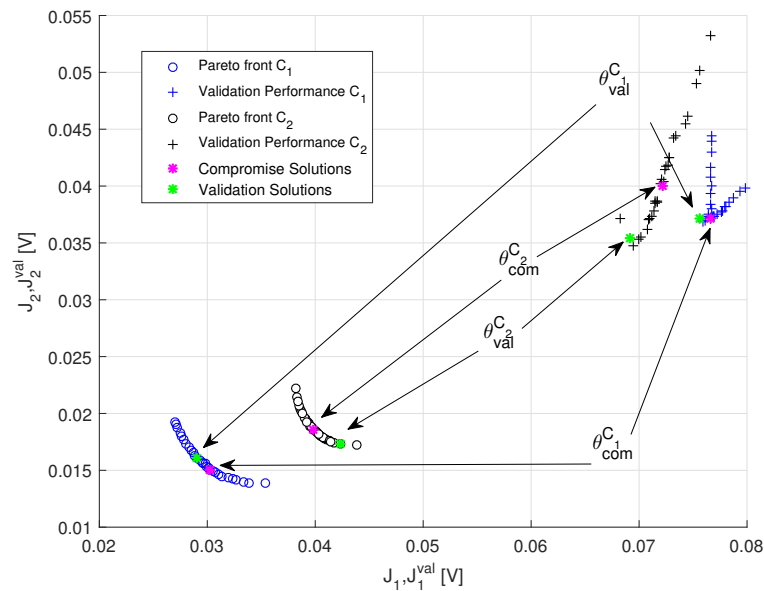

Figure 14. Pareto solutions obtained from the identification data and their performances in the validation test. The compromise and validation solutions are highlighted.

Figures 15–17 show the responses of the previously mentioned solutions (θ_{val}^{C1} and θ_{val}^{C2}) in three different tests, namely, a discharge test, a charge test and the validation test. In the discharge test, both responses were quite similar, except in $Zone_{LSOC}$, where the complete model was more accurate.
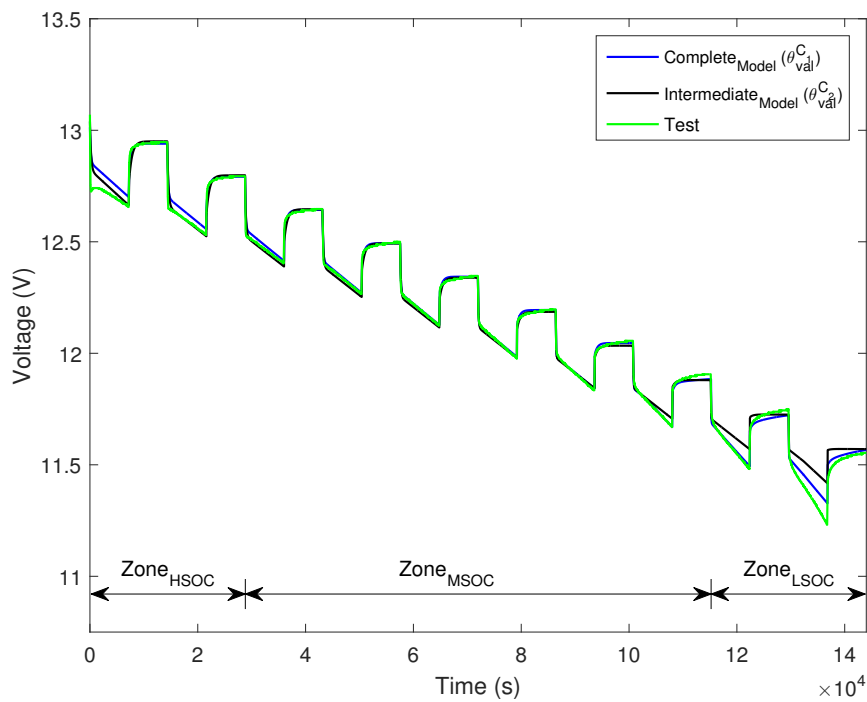

Figure 15. $\theta_{val}^{C_1}$ and $\theta_{val}^{C_2}$ responses in test 3.
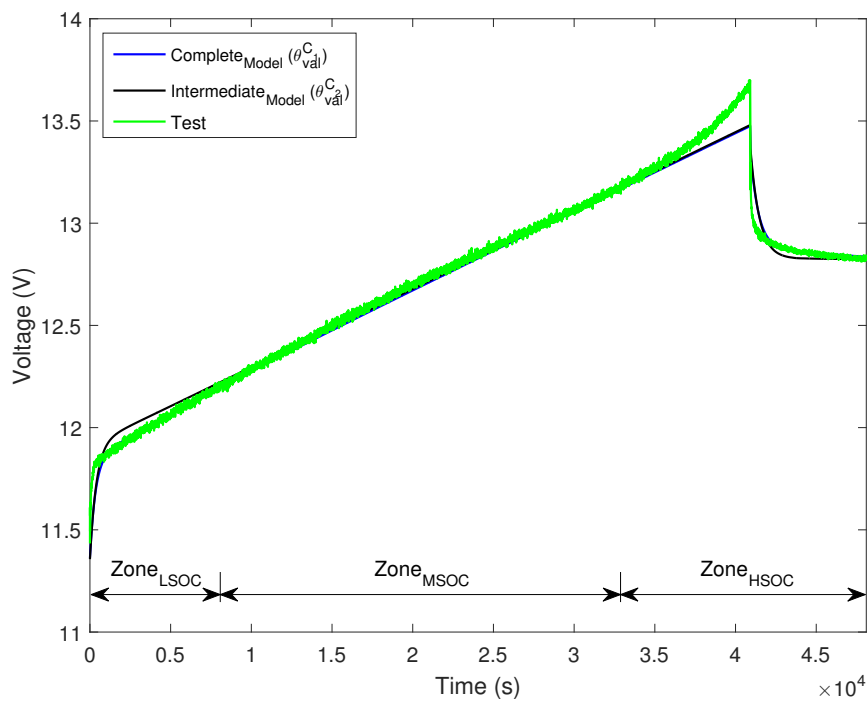

Figure 16. $\theta_{val}^{C_1}$ and $\theta_{val}^{C_2}$ responses in test 4.

In the charge test, both responses were similar as well. Finally, in the validation test, again, both responses resembled each other, although the intermediate model had less error. Let us analyze these results in a more detailed way. In $Zone_{MSOC}$ (J_2), both responses were similar. In $Zone_{LSOC}$, the intermediate model performed worse than the complete model, as expected. However, in $Zone_{HSOC}$, the intermediate model performed better than the complete model. This better matching in $Zone_{HSOC}$ compensated for the poor matching in $Zone_{LSOC}$, which led to an improvement in J_1 (low and high SOC zones), that is to say, a better performance with respect to this objective. The only zone where the intermediate model was worse than the complete model in all the tests was $Zone_{LSOC}$, but this zone was the least interesting, as it was not recommended for discharging a battery fully. In the rest of the zones, the discrepancies between the model and the experimental data were negligible. All the errors in all the tests were within $\pm$ 2.5% of the battery voltage. Similar figures were achieved in [17,22]. Consequently, the results were acceptable. As a result of the previous analysis, the intermediate model was finally chosen as the best solution, as it reduced complexity, while barely losing performance, and even improved the response in the validation test. This solution was $\theta_{val}^{C_2}$ (Table 5).
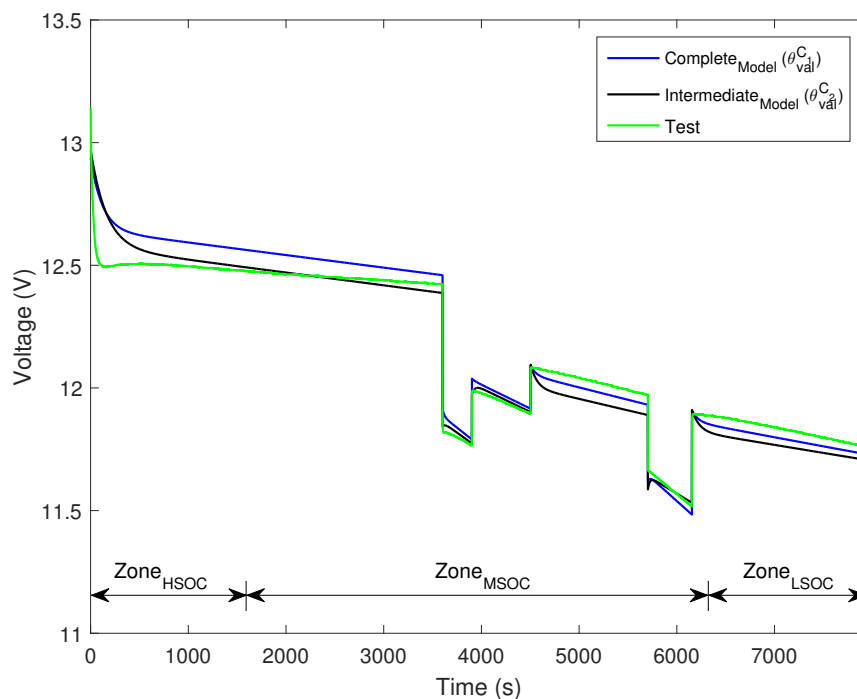

Figure 17. $\theta_{val}^{C_1}$ and $\theta_{val}^{C_2}$ responses in the validation test.

Table 5. Values of each parameter of the chosen solution ($\theta_{val}^{C_2}$).

Parameter	Value	Parameter	Value	Parameter	Value	Parameter	Value
K_e^h	6.55×10^{-3}	K_e^m	6.59×10^{-3}	K_e^l	6.19×10^{-3}	K_e^c	9.08×10^{-3}
R_{00}^h	0.0251	R_{00}^m	0.0323	R_{00}^l	0.0385	A_0^h	0.12
A_0^m	0.703	A_0^l	1.36	R_{11}	0.0119	R_{12}	1×10^{-5}
R_{13}	0.0253	R_{14}	8×10^{-4}	R_{15}	0.139	R_{16}	0.0129
R_{17}	-0.0581	R_{18}	0.399	C_a	1.43×10^3	–	–

6. Conclusions

In this paper, a methodology for the analysis of different concepts through a multiobjective approach was presented. A concept is a way of solving a problem. The use of concepts, combined

with multiobjective techniques, enables a designer to simultaneously compare the performance of various design concepts with respect to the desired objectives. As an example of an application, this methodology was applied to the development of a battery model. Thanks to the direct comparison of different concepts that the multiobjective approach provided, the designer was able to assess the performance of three different model structures, each of them with distinct degrees of complexity. By taking into account two desired objectives (model matching to empirical data in low, medium and high SOC zones) and evaluating the model degradation in the validation data, the designer managed to achieve a comprehensive perspective, so that they could make an informed decision and select the best solution according to their preferences. The decision-making process, in our example, resulted in choosing the intermediate model structure, as it was simpler than the complete structure, and demonstrated a better performance in the validation test.

Author Contributions: Raul Simarro performed the experimental tests and revised the manuscript. Juan Manuel Herrero, Xavier Blasco and Alberto Pajares developed the battery models, and defined and solved the multiobjective optimization problem (MOP). All the authors participated in the data analysis, as well as in the writing of the paper.

Conflicts of Interest: The authors declare no conflict of interest.

References

1. Mattson, C.A.; Messac, A. Concept selection using s-Pareto frontiers. *AIAA J.* **2003**, *41*, 1190–1198.
2. Mattson, C.A.; Messac, A. Pareto frontier based concept selection under uncertainty, with visualization. *Optim. Eng.* **2005**, *6*, 85–115.
3. Chang, W.Y. The state of charge estimating methods for battery: A review. *ISRN Appl. Math.* **2013**, *2013*, doi:10.1155/2013/953792.
4. Lee, D.T.; Shiah, S.J.; Lee, C.M.; Wang, Y.C. State-of-charge estimation for electric scooters by using learning mechanisms. *IEEE Trans. Veh. Technol.* **2007**, *56*, 544–556.
5. Hua, C.C.; Tasi, T.Y.; Chuang, C.W.; Shr, W.B. Design and implementation of a residual capacity estimator for lead-acid batteries. In Proceedings of the 2nd IEEE Conference on Industrial Electronics and Applications, Harbin, China, 23–25 May 2007; pp. 2018–2023.
6. Ramadass, P.; Haran, B.; Gomadam, P.M.; White, R.; Popov, B.N. Development of first principles capacity fade model for Li-ion cells. *J. Electrochem. Soc.* **2004**, *151*, A196–A203.
7. Sanchis, J.; Martínez, M.A.; Blasco, X. Integrated multiobjective optimization and a priori preferences using genetic algorithms. *Inf. Sci.* **2008**, *178*, 931–951.
8. Reynoso-Meza, G.; Sanchis, J.; Blasco, X.; Freire, R.Z. Evolutionary multi-objective optimisation with preferences for multivariable PI controller tuning. *Expert Syst. Appl.* **2016**, *51*, 120–133.
9. Herrero, J.; Blasco, X.; Martínez, M.; Ramos, C.; Sanchis, J. Non-linear robust identification of a greenhouse model using multi-objective evolutionary algorithms. *Biosyst. Eng.* **2007**, *98*, 335–346.
10. Deb, K.; Sindhya, K.; Hakanen, J. Multi-objective optimization. In *Decision Sciences: Theory and Practice*; CRC Press: Boca Raton, FL, USA, 2016; pp. 145–184.
11. Miettinen, K. Nonlinear Multiobjective Optimization. In *International Series in Operations Research and Management Science*, 12nd ed.; Spring: Berlin, Germany, 1999.
12. Bonissone, P.P.; Subbu, R.; Lizzi, J. Multicriteria decision making (MCDM): A framework for research and applications. *IEEE Comput. Intell. Mag.* **2009**, *4*, 48–61.
13. Reynoso-Meza, G.; Blasco, X.; Sanchis, J.; Herrero, J.M. Comparison of design concepts in multi-criteria decision-making using level diagrams. *Inf. Sci.* **2013**, *221*, 124–141.
14. Coello, C.A.C.; Lamont, G.B. *Applications of Multi-Objective Evolutionary Algorithms*, 1st ed.; World Scientific: Singapore, 2004.
15. You, D.; Zhang, H.; Chen, J. A simple model for the vanadium redox battery. *Electrochimica Acta* **2009**, *54*, 6827–6836.

16. Chen, M.; Rincon-Mora, G.A. Accurate electrical battery model capable of predicting runtime and IV performance. *IEEE Trans. Energy Convers.* **2006**, *21*, 504–511.

17. Malik, A.; Zhang, Z.; Agarwal, R.K. Extraction of battery parameters using a multi-objective genetic algorithm with a non-linear circuit model. *J. Power Sources* **2014**, *259*, 76–86.

18. Burgos, C.; Sáez, D.; Orchard, M.E.; Cárdenas, R. Fuzzy modelling for the state-of-charge estimation of lead-acid batteries. *J. Power Sources* **2015**, *274*, 355–366.

19. Xu, L.; Wang, J.; Chen, Q. Kalman filtering state of charge estimation for battery management system based on a stochastic fuzzy neural network battery model. *Energy Convers. Manag.* **2012**, *53*, 33–39.

20. Tremblay, O.; Dessaint, L.A.; Dekkiche, A.I. A generic battery model for the dynamic simulation of hybrid electric vehicles. In Proceedings of the Vehicle Power and Propulsion Conference, Arlington, TX, USA, 9–12 September 2007; pp. 284–289.

21. Einhorn, M.; Conte, F.V.; Kral, C.; Fleig, J. Comparison, selection, and parameterization of electrical battery models for automotive applications. *IEEE Trans. Power Electron.* **2013**, *28*, 1429–1437.

22. Tremblay, O.; Dessaint, L.A. Experimental validation of a battery dynamic model for EV applications. *World Electr. Veh. J.* **2009**, *3*, 1–10.

23. Wang, J.; Cao, B.; Chen, Q.; Wang, F. Combined state of charge estimator for electric vehicle battery pack. *Control Eng. Pract.* **2007**, *15*, 1569–1576.

24. Moubayed, N.; Kouta, J.; El-Ali, A.; Dernayka, H.; Outbib, R. Parameter identification of the lead-acid battery model. In Proceedings of the 33rd IEEE Photovoltaic Specialists Conference, San Diego, CA, USA, 11–16 May 2008; pp. 1–6.

25. Ceraolo, M. New dynamical models of lead-acid batteries. *IEEE Trans. Power Syst.* **2000**, *15*, 1184–1190.

26. Reynoso-Meza, G.; Garcia-Nieto, S.; Sanchis, J.; Blasco, F.X. Controller tuning by means of multi-objective optimization algorithms: A global tuning framework. *IEEE Trans. Control Syst. Technol.* **2013**, *21*, 445–458.

27. Herrero, J.; Reynoso-Meza, G.; Martínez, M.; Blasco, X.; Sanchis, J. A smart-distributed Pareto front using the ev-MOGA evolutionary algorithm. *Int. J. Artif. Intell. Tools* **2014**, *23*, 1450002.

28. Herrero, J.M.; García-Nieto, S.; Blasco, X.; Romero-García, V.; Sánchez-Pérez, J.V.; Garcia-Raffi, L. Optimization of sonic crystal attenuation properties by ev-MOGA multiobjective evolutionary algorithm. *Struct. Multidiscip. Optim.* **2009**, *39*, 203.

29. Herrero, J.; Blasco, X.; Sánchez-Pérez, J.; Redondo, J. Design of sound phase diffusers by means of multiobjective optimization approach using ev-MOGA evolutionary algorithm. *Struct. Multidiscip. Optim.* **2016**, *53*, 861–879.